RSC Advances

PAPER

View Article Online
View Journal | View Issue

Cite this: *RSC Adv.*, 2019, **9**, 24171

Highly efficient crystallization of $AlPO_4$-5 accelerated by a rotating hydrothermal synthesis route†

Kun Xia, Zhechao He, Dan Zhou, * Xinhuan Lu and Qinghua Xia *

Received 27th June 2019
Accepted 25th July 2019

DOI: 10.1039/c9ra04842a

rsc.li/rsc-advances

Compared with static hydrothermal synthesis, the crystallization rate of an $AlPO_4$-5 molecular sieve has been accelerated distinctly by a rotating hydrothermal synthesis route with obviously decreased crystal particle size, which is assumed to be ascribed to the increased nucleation centers, accelerated crystal nucleation and growth processes; five-coordinated Al is dominant in the initial reaction gel, and the assembly from amorphous Al species to long-range ordered crystals is mainly contributed by the conversion from five-coordinated Al to four-coordinated Al.

Zeolites and molecular sieves, an important class of microporous crystal materials, have wide applications in chemical industry as the most important sorbent and separator, ion exchanger, catalyst, and functional materials.[1–6] Various methods have been developed to synthesize zeolites with novel structure, tunable composition, and unique morphology based on different applications.

For the consideration of sustainable development and energy conservation, rapid and efficient synthesis of zeolite materials has aroused great interest. Various methods, such as microwave-assisted hydrothermal,[7,8] ultrasound-assisted hydrothermal,[9,10] and seed-assisted synthesis methods,[11–13] have been proven to be efficient for promoting the synthesis of zeolite. Moreover, hydroxyl free radicals are also found to have important influence on accelerating the crystallization of zeolites.[14,15] Recently, rotating synthesis route is found to be efficient for the fast crystallization of zeolites and can result in different crystal morphology and size.[16–18] It is noteworthy that there are no stirring devices such as stirring blades (rods, propellers) and no stirrers in the 'rotating' crystallization device. Although the research on the crystallization process of molecular sieves under static or dynamic stirring condition has been reported, the crystallization process under 'rotating' condition is not reported systematically.

Herein, fast crystallization of $AlPO_4$-5 is successfully realized by rotating hydrothermal method (Fig. S1†), and the crystallization process of which has been discussed systematically. Compared with static hydrothermal route, both the nucleation and growth processes have been accelerated distinctly. Moreover, five-coordination Al species in the initial reaction gel is the dominant Al species. The conversion from amorphous phase to AFI crystal phase accompanies the fast conversion from five-coordination state Al species to four-coordination state Al species accelerated by rotating effect, different from static hydrothermal synthesis route.

Rotating hydrothermal synthesis of $AlPO_4$-5 is conducted under different rotation rate level, and powder XRD measurement is employed to monitor the crystallization of $AlPO_4$-5. As shown in Fig. 1, obvious AFI diffraction peaks have been observed for samples R-180(30)-20, R-180(30)-60, R-180(30)-100, and R-180(30)-140. Noticeably, crystallization at 180 °C for

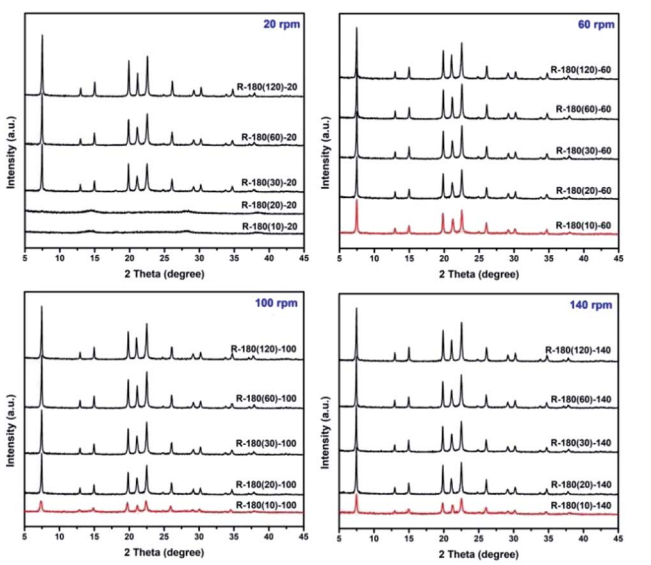

Fig. 1 Powder XRD patterns of $AlPO_4$-5 prepared by rotating hydrothermal route.

Ministry-of-Education Key Laboratory for the Synthesis and Application of Organic Functional Molecules, Hubei University, Wuhan 430062, China. E-mail: d.zhou@hubu.edu.cn; xiaqh518@aliyun.com

† Electronic supplementary information (ESI) available. See DOI: 10.1039/c9ra04842a

20 min is not enough for the formation of AFI phase under rotation rate of 20 rpm (sample R-180(20)-20), but sufficient under rotation rate of 60–140 rpm (sample R-180(20)-60, R-180(20)-100, and R-180(20)-140). Surprisingly, by crystallization at 180 °C for merely 10 min under rotation rate of 60–140 rpm, obvious AFI diffraction peaks have emerged, which has been verified by repeated experiments. Obviously, the crystallization time for the formation of long-range ordered crystal structure from amorphous phase has been shortened distinctly, and relatively higher rotating rate of the autoclave (60–140 rpm) is believed to play an important role in accelerating the crystallization of $AlPO_4$-5.

The morphology of $AlPO_4$-5 samples by rotating hydrothermal method is illustrated in Fig. 2 and S2 (ESI).† For sample R-180(10)-60, the majority of particles are cylindrical morphology, and the particle size is in the range from 1.3 to 5.0 μm. The mixture of smaller crystal particles and aggregation are observed for sample R-180(10)-100. For sample R-180(10)-140, the mixture of small particles without regular shape and aggregation are observed, similar to that of sample R-180(10)-100.

The XRD patterns of $AlPO_4$-5 samples synthesized by static hydrothermal method are shown in Fig. S3(a).† No AFI diffraction peak is observed for sample S-180(30). Weak AFI diffraction peaks are observed when heating the gel at 180 °C for 45 min (sample S-180(45)). The morphology of samples S-180(45) and S-180(60) are the mixture of spherical crystal particles and amorphous phase, and samples S-180(120) and S-180(180) are well-crystallized spherical crystal particles, as shown in Fig. S3(b).†

In addition, crystallization temperature is also investigated for the synthesis of $AlPO_4$-5 under rotation rate of 60 rpm, and the powder XRD patterns are shown in Fig. S4.† The relative crystallinity of $AlPO_4$-5 calculated (based on the XRD diffraction peaks in Fig. S5†) as a function of the crystallization time at specified crystallization temperatures is shown in Fig. S6.† When the temperature is higher than 170 °C, crystallization rate has been increased sharply. Moreover, the conversion from amorphous phase to ordered crystal structure under 180–190 °C happened between 8 and 10 min, during which about 72–76% relative crystallinity have been contributed in merely a period of 2 min. However, the following period of 50 min (between 10 and 60 min) only contributes about 28% and 24% relative crystallinity of $AlPO_4$-5 under 180 °C and 190 °C, respectively.

The comparison of relative crystallinity of samples synthesized under rotating and static condition as a function of crystallization time is shown in Fig. 3. Under rotation rate of 60 rpm, heating the reaction gel for a period of 52 min (from 8 to 60 min) can contribute 100% relative crystallinity of $AlPO_4$-5; however, under static condition, a period of 1400 min (from 40 to 1440 min) contributes only about 96% relative crystallinity of $AlPO_4$-5. Based on the crystallization rate, the growth of crystal can be divided into two stages: Stage I, 72% contribution to relative crystallinity; Stage II, 28% contribution to relative crystallinity. The comparison of crystallization rate between rotating and static synthesis shows that the heating time for the contribution of 100% relative crystallinity under rotating condition is about 1/27 (52/1400) of that under static condition, suggesting the high efficiency of rotating synthesis.

Because of the T–O–T (T, tetrahedral site) bending vibrations being sensitive to the ring structures in zeolite framework, the Raman spectra of samples prepared under rotation rate of 60 rpm at various stages were recorded. As shown in Fig. 4, a weak peak at 498 cm^{-1} is observed for initial reaction gel, which is ascribed to 4-membered ring (4-MR) structure.[19] It implies that 4-MRs have formed in amorphous phase. Samples R-180(5)-60 and R-180(8)-60 have the similar peaks with that of R-180(0)-60. When the heating time at 180 °C is prolonged to 9 min (sample R-180(9)-60), the intensity of the peaks at 498 cm^{-1} and at 412 cm^{-1} increase significantly, and one peak at 260 cm^{-1} emerges, which is attributed to the 12-

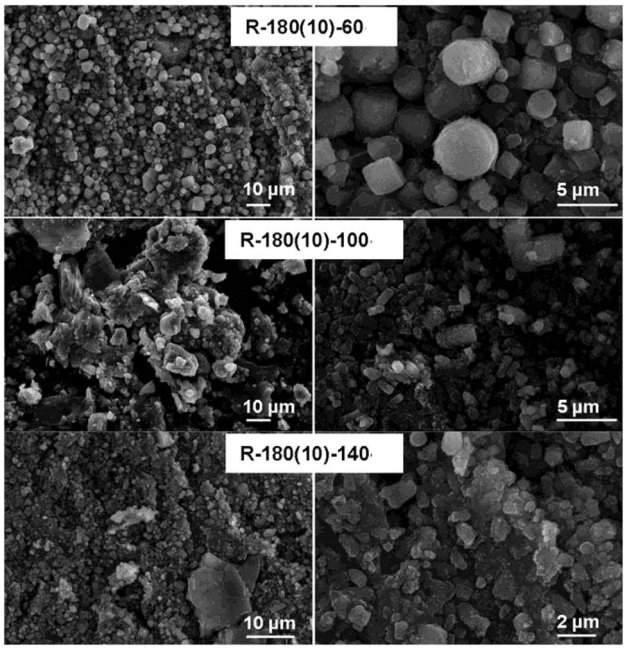

Fig. 2 SEM images of $AlPO_4$-5 prepared under rotating hydrothermal condition (heating the gel at 180 °C for 10 min).

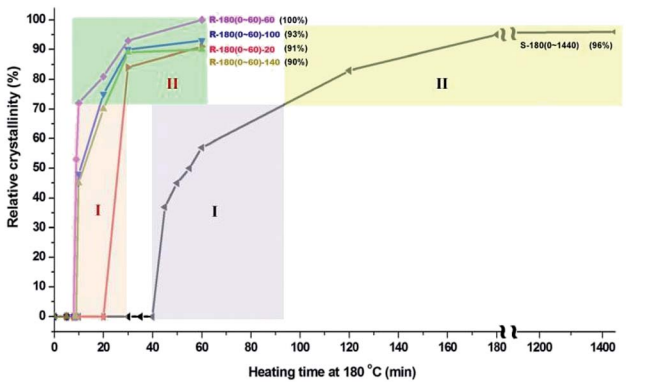

Fig. 3 Comparison of relative crystallinity of samples synthesized under rotating and static condition as a function of heating time at 180 °C.

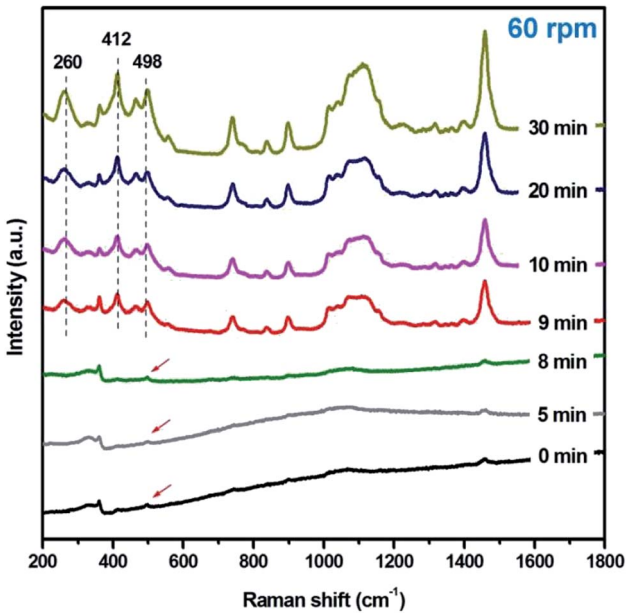

Fig. 4 Raman spectra of $AlPO_4$-5 prepared under rotation rate of 60 rpm.

MR structure. As the crystallization time is increased from 9 to 30 min, the intensity of these three peaks (498, 412, and 260 cm^{-1}) is gradually enhanced, suggesting that 12-MR, 6-MR and 4-MR structures are well constructed through the transformation of amorphous species.

Local chemical environments of Al and P atoms in the samples prepared under rotating condition at various stages were further investigated by solid-state ^{27}Al and ^{31}P MAS NMR measurements. As shown in the ^{27}Al MAS NMR spectra (Fig. 5, left), one signal at 7 ppm and two broad signals at 38 and

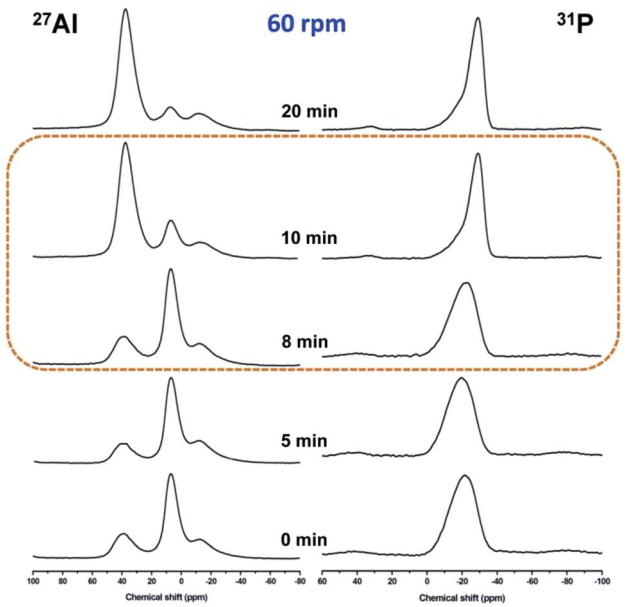

Fig. 5 Solid-state ^{27}Al and ^{31}P MAS NMR spectra of as-synthesized $AlPO_4$-5 under rotation speed of 60 rpm.

−12 ppm are observed for the initial reaction gel, which is respectively assigned to five-coordinated Al species $Al(OP)_4(-OH_2)$, four-coordinated Al species $Al(OP)_4$, and six-coordinated Al species $Al(OP)_4(OH_2)_2$, respectively.[20–22] The percentage of various Al coordinated states determined by quantitative data of ^{27}Al MAS NMR spectra is listed in Table S4.† Obviously, the five-coordinated Al species are prominent, which is about 70% of the total Al species in the sample. This is different from the static hydrothermal synthesis route[23] and DGC route[24] reported, in which four-coordinated Al is prominent. It implies that the stable coordination state of Al species in the initial reaction gel is influenced by the crystallization routes;[23–25] five-coordinated $Al(OP)_4(OH_2)$ species is more easier to be formed under rotating hydrothermal condition, for comparison, four-coordinated $Al(OP)_4$ is easier to be formed under static synthesis route, including static "hydrothermal or DGC" route. The peak shape of ^{27}Al MAS NMR spectra for samples R-180(5)-60 and R-180(8)-60 has no obvious difference with that of starting reaction gel, implying that intermediate phases R-180(5)-60 and R-180(8)-60 have the similar Al chemical environment with that of initial gel. However, different peak shape is shown in the spectrum of R-180(10)-60, in which prominent Al species is four-coordinated Al (*ca.* 82%). The percentage of four-coordinated Al in sample R-180(20)-60 reaches the maximum (*ca.* 87%). From the quantitative data listed in Table S4,† the percentage of six-coordinated Al in all samples is lower than 6.5%. Based on the above analysis, it is assumed that the assembly from amorphous Al species to long-range ordered crystals with AFI framework is mainly contributed by the conversion from five-coordinated Al to four-coordinated Al.

The ^{31}P MAS NMR spectra of the corresponding samples are shown in Fig. 5 (right). A broad resonance centered at around −21 ppm is observed in the ^{31}P MAS NMR spectra of R-180(0)-60, R-180(5)-60 and R-180(8)-60, implying the similar chemical environment of P with wide distribution, consistent with the amorphous nature of the materials. In the ^{31}P MAS NMR spectrum of R-180(10)-60, a narrow peak centered at around −29 ppm is observed, which is ascribed to $P(OAl)_4$ environment and consistent with the reported result.[20–22] The ^{31}P MAS NMR peak shape of R-180(20)-60 looks nearly identical with that of R-180(10)-60, which is consistent with the reported results,[23–25] implying that R-180(10)-60 has the similar P chemical environment with well-crystallized $AlPO_4$-5 (R-180(20)-60).

Based on the above analysis, the conversion from amorphous phase to long-range ordered crystals under rotating hydrothermal condition can be completed in minute scale, different from the crystallization process of $AlPO_4$-5 prepared by other methods, inclusive of static hydrothermal method,[23] DGC,[24] and solvent-free synthesis.[25] The crystallization process of $AlPO_4$-5 under rotating hydrothermal route in time scale is shown in Fig. 6. Based on the liquid phase transition mechanism,[26] the formation of nuclei and the formation of zeolite crystals both result from the reaction of some species (Al species and P species in this work) dissolved in the liquid phase of the reaction mixture and derived from the amorphous substrate; compared with static crystallization mode, rotating crystallization mode probably accelerates the dissolution and derivation

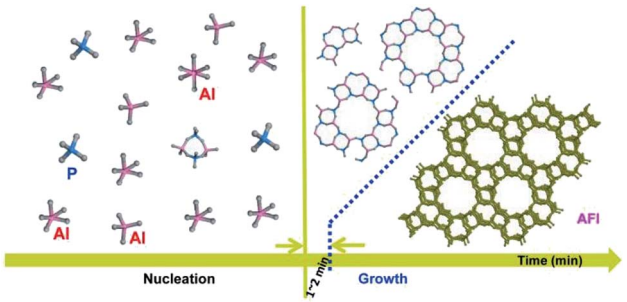

Fig. 6 Crystallization process of $AlPO_4$-5 under rotating hydrothermal route.

process, which enhances the crystallization process consequently.

Conclusions

Rapid synthesis of $AlPO_4$-5 molecular sieve is successfully realized by rotating hydrothermal route, which is proven to be an efficient, time-saving and energy-conservation method. Different from static hydrothermal synthesis, five-coordinated Al species is dominant in the reaction gel prepared by rotating hydrothermal route, and the assembly from amorphous Al species to long-range ordered crystals is mainly contributed by the conversion from five-coordinated Al to four-coordinated Al. The high crystallization efficiency of $AlPO_4$-5 under rotating condition is assumed to be ascribed to the increased nucleation centers, accelerated crystal nucleation and growth processes.

Conflicts of interest

There are no conflicts to declare.

Acknowledgements

The authors thank the financial supports by National Natural Science Foundation of China (21571055, 21673069, 21503074), Hubei Province Outstanding Youth Foundation (2016CFA040), Ministry-of-Education Key Laboratory for the Synthesis and Application of Organic Functional Molecules (KLSAOFM1808), Applied Basic Frontier Project of Wuhan Science and Technology Bureau (2019010701011415), and the technical supports by State Center for Magnetic Resonance in Wuhan for the solid-state NMR experiments.

Notes and references

1 R. R. Xu, W. Q. Pang, J. H. Yu, Q. S. Huo and J. S. Chen, *Chemistry of zeolites and related porous materials*, Wiley-VCH, Singapore, 2007.
2 C. G. Li, M. Moliner and A. Corma, *Angew. Chem., Int. Ed.*, 2018, **57**, 15330–15353.
3 M. Dusselier and M. E. Davis, *Chem. Rev.*, 2018, **118**, 5265–5329.
4 L. H. Chen, X. Y. Li, G. Tian, Y. Li, J. C. Rooke, G. S. Zhu, S. L. Qiu, X. Y. Yang and B. L. Su, *Angew. Chem., Int. Ed.*, 2011, **50**, 11156–11161.
5 C. Wang, M. Yang, P. Tian, S. T. Xu, Y. Yang, D. H. Wang, Y. Y. Yuan and Z. M. Liu, *J. Mater. Chem. A*, 2015, **3**, 5608–5616.
6 Y. Zhao, D. Zhou, T. Zhang, Y. Yang, K. Zhan, X. Liu, H. Min, X. Lu, R. Nie and Q. Xia, *ACS Appl. Mater. Interfaces*, 2018, **10**, 6390–6397.
7 W. Yan, E. W. Hagaman and S. Dai, *Chem. Mater.*, 2004, **16**, 5182–5186.
8 X. Zhao, J. Zhao, J. Wen, A. Li, G. Li and X. Wang, *Microporous Mesoporous Mater.*, 2015, **213**, 192–196.
9 E.-P. Ng, H. Awala, J.-P. Ghoy, A. Vicente, T. C. Ling, Y. H. Ng, S. Mintova and F. Adam, *Mater. Chem. Phys.*, 2015, **159**, 38–45.
10 S. S. Zhuang, Z. J. Hu, L. Huang, F. Qin, Z. Huang, C. Sun, W. Shen and H. L. Xu, *Catal. Commun.*, 2018, **114**, 28–32.
11 K. Itabashi, Y. Kamimura, K. Iyoki, A. Shimojima and T. Okubo, *J. Am. Chem. Soc.*, 2012, **134**, 11542–11549.
12 H. L. Zhou, Y. J. Wu, W. Zhang and J. Wang, *Mater. Chem. Phys.*, 2012, **134**, 651–656.
13 Y. Yang, T. Zhang, D. Zhou, X. Liu, S. Yang, X. Lu and Q. Xia, *Mater. Chem. Phys.*, 2019, **236**, 121754.
14 G. Feng, P. Cheng, W. Yan, M. Boronat, X. Li, J. Su, J. Wang, Y. Li, A. Corma, R. Xu and J. Yu, *Science*, 2016, **351**, 1188–1191.
15 P. Cheng, G. Feng, C. Sun, W. Xu, J. Su, W. Yan and J. Yu, *Inorg. Chem. Front.*, 2018, **5**, 2106–2110.
16 D. Zhou, T. Zhang, Q. H. Xia, Y. R. Zhao, K. Lv, X. Lu and R. Nie, *Chem. Sci.*, 2016, **7**, 4966–4972.
17 K. Xia, D. Zhou, Y. Yang, S. Yang and Q. Xia, *Chem. Res. Chin. Univ.*, 2018, **39**, 1624–1630.
18 D. Li, Z. Wu, D. Zhou, Y. Xia, X. Lu, H. He and Q. Xia, *Microporous Mesoporous Mater.*, 2019, **280**, 195–202.
19 F. Fan, Z. Feng, K. Sun, M. Guo, Q. Guo, Y. Song, W. Li and C. Li, *Angew. Chem., Int. Ed.*, 2009, **48**, 8743–8747.
20 J. Xu, Q. Wang, S. Li and F. Deng, *Solid-state NMR in zeolite catalysis*, Wiley-VCH, Springer Nature Singapore Pte Ltd., 2019.
21 A. Wang, J. Xu, C. Wang, F. Deng, R. Xu and W. Yan, *Chem. Res. Chin. Univ.*, 2017, **33**, 513–519.
22 Y. Tian, J. Xu, Z. Wang, F. Deng, R. Xu and W. Yan, *Chem. Res. Chin. Univ.*, 2017, **33**, 853–859.
23 J. G. Longstaffe, B. Chen and Y. Huang, *Microporous Mesoporous Mater.*, 2007, **98**, 21–28.
24 B. Chen, C. W. Kirby and Y. Huang, *J. Phys. Chem. C*, 2009, **113**, 15868–15876.
25 N. Sheng, Y. Chu, S. Xin, Q. Wang, X. Yi, Z. Feng, X. Meng, X. Liu, F. Deng and F. Xiao, *J. Am. Chem. Soc.*, 2016, **138**, 6171–6176.
26 G. T. Kerr, *J. Phys. Chem.*, 1966, **70**, 1047–1050.